Biomedical Materials

PAPER

Injectable β-TCP/MCPM cement associated with mesoporous silica for bone regeneration: characterization and toxicity evaluation

Biomedical Materials

PAPER

Injectable β-TCP/MCPM cement associated with mesoporous silica for bone regeneration: characterization and toxicity evaluation

RECEIVED
4 May 2017

REVISED
27 September 2017

ACCEPTED FOR PUBLICATION
3 October 2017

PUBLISHED
8 February 2018

L S Mendes[1], S Saska[1], F Coelho[2], T S de O Capote[2], R M Scarel-Caminaga[2], R Marchetto[1], R G Carrodeguas[3], A M M Gaspar[2] and M A Rodríguez[4]

[1] São Paulo State University (Unesp), Institute of Chemistry, Araraquara, SP, Brazil
[2] São Paulo State University (Unesp), School of Dentistry, Araraquara, SP, Brazil
[3] Azurebio S.L., Madrid, Spain
[4] Instituto de Cerámica y Vidrio, CSIC, Madrid, Spain

E-mail: la_mendes@hotmail.com

Keywords: calcium phosphate cement, mesoporous silica, injectability, bioactivity, toxicity analysis, bone repair

Abstract

Calcium phosphate cement has been widely investigated as a bone graft substitute due to its excellent self-setting ability, biocompatibility, osteoconductivity and moldability. In addition, mesoporous materials have been studied as potential materials for application in medical devices due to their large surface area, which is capable of loading numerous biological molecules, besides being bioactive. In this study, bone β-TCP-MCPM-based injectable cement with mesoporous silica particles was synthesized and characterized in terms of its mechanical properties, microstructure, porosity, injectability, *in vitro* bioactivity and degradability; together with toxicity effects in CHO-K1 cell culture. The results showed that the β-TCP-MCPM cement is bioactive after soaking in simulated body fluid solution, and mesoporous silica particles provided better physicochemical properties compared with silica-free cement. Toxicity assays showed low CHO-K1 cell viability after treatment with more concentrated extracts (200 mg ml^{-1}). However, this behavior did not compromise the reproductive capacity and did not promote significant DNA damage in those cells. In conclusion, the β-TCP-MCPM cement associated with mesoporous silica might be considered as a potential bone substitute for the repair and regeneration of bone defects.

1. Introduction

Calcium phosphate biomaterials have been widely used as bone substitute materials in clinical applications due to their higher similarity to biological apatites, their biocompatibility and osteoconductive property [1]. Clinical procedures such as minimally invasive surgery for the replacement/reconstruction of irregular-shaped bone defects have some limitations to the application of sintered bioactive ceramics [2]. In this context, calcium phosphate cements (CPCs) have been widely explored as a good alternative synthetic graft. CPC can be molded or injected to be used as bone defect filler in maxillofacial surgery and in orthopedic fracture treatment in order to conform to the shape of the bone defect surface [3].

CPC consists of a powder and a liquid phase, which forms a moldable paste upon mixing. After that, these compounds set and the final product may be brushite (dicalcium phosphate dihydrate, DCPD) or hydroxyapatite (HA) depending on factors such as the pH of the setting and thermodynamic stability [4]. DCPD cements have raised interest, because they are metastable under physiological conditions, and for this reason can be resorbable more quickly than apatite-forming cements, showing excellent degradability and enhanced bone formation *in vivo* [5].

DCPD cements are obtained as a result of an acid-base reaction, most of them containing β-TCP and an acid component, usually monocalcium phosphate monohydrate (MCPM) or phosphoric acid [6]. Within the group of DCPD cements, the type formed by the combination of β-TCP and MCPM [7] shows relatively rapid setting when mixed with water (around 30 s). To avoid this problem, the phosphate salts can be mixed with non-aqueous but water-miscible liquid, which can increase the curing time, as well as the injectability of the paste cement [8].

Since the first report about bone cements in the 1980s [9, 10], new cement formulations have been developed for applications such as bone filling [11, 12], bone reinforcement in osteoporosis [13], fixation of metal implants [14], vertebral column fractures and vertebroplasty [15].

In recent years, many studies have focused on combining materials with potential in bone repair to promote different therapeutic approaches, such as association with materials capable of incorporating drugs or other therapeutically relevant molecules. In this context, mesoporous silica has been highlighted in the development of materials for bone repair, due to its high surface area and porosity, besides its excellent biological properties, such as compatibility and bioactivity [16, 17] that allow these particles to be used as potential carriers of biologically active molecules such as drugs, proteins, peptides and enzymes [18–21].

Since the discovery of Bioglass® [22], many bioactivity studies have been carried out on biomaterials containing silica in physiological fluids [23, 24], showing that porosity and specific surface area play an important role in the bioactivity of material. In addition, a surface with negative charges due to the high density of the silanol groups (Si–OH) on the silica surface is the key element to induce the nucleation of HA [25–27]. Thus, the addition of mesoporous silica particles can be used to increase the bone repair capacity of the CPCs [28, 29].

Therefore, this study was aimed at the synthesis of a βTCP-MCPM-based injectable cement with mesoporous silica particles as a possible candidate for application in bone repair/regeneration. The injectable cements were characterized in terms of their mechanical properties and microstructure, porosity, injectability, *in vitro* bioactivity and degradability. Moreover, *in vitro* assays evaluated whether they exhibited cytotoxic, genotoxic and mutagenic effects in CHO-K1 cell culture.

2. Materials and methods

2.1. Synthesis of mesoporous silica

The mesoporous silica was synthesized in accordance with our previous study [30]. Mesoporous silica particles were synthesized from solutions containing a block copolymer as the structure-directing agent (non-ionic surfactant P123 (Pluronic® 123, $EO_{20}PO_{70}EO_{20}$,Sigma-Aldrich®) and tetraethylorthosilicate (TEOS, $Si(CH_3CH_2O)_4$, Sigma-Aldrich®) as a source of silica. The surfactant was removed by a calcination method at 600 °C for 6 h. Silica particles showed periodic arrangement of parallel channels typical of mesoporous materials with a hexagonal arrangement, with a pore size of 60 Å, high surface area (880 m^2 g^{-1}) and around 462 nm length [30].

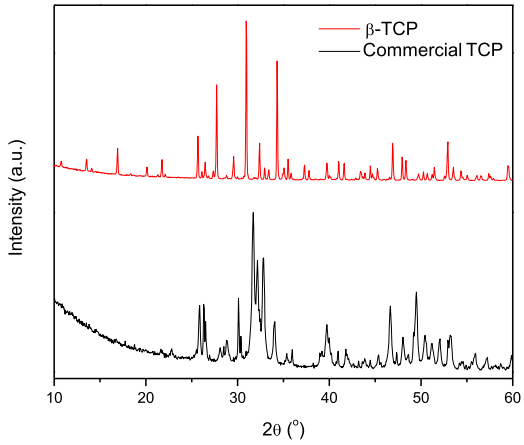

Figure 1. XRD patterns of commercial TCP before and after heat treatment at 1100 °C.

2.2. Preparation of the cements

First, β-TCP was obtained by heating tricalcium phosphate RPH (Carlo Erba Reagents) in a furnace at 1100 °C for 4 h. The material obtained was crushed, sieved under 63 μm and β-TCP was confirmed by x-ray diffraction (XRD) analysis (figure 1). MCPM as the analytical-grade reagent was used as supplied (Sigma-Aldrich®). Then, the βTCP-MCPM cement was prepared by premixing (2:1 molar ratio), according to table 1. The β-TCP/MCPM ratio was calculated in order to obtain theoretically a β-TCP content of 67%. Each formulation, without (β-TCP/MCPM) or with 5 wt% silica (β-TCP/MCPM/Si), was prepared by mixing the powder to liquid with the aid of a spatula for 3 min in a glass plate. A solution of polyethylene glycol 400 (PEG 400, Sigma-Aldrich®) and deionized water (1:1, v/v) was used as the liquid component in the preparation of the cements. The best ratio liquid/powder (L/P) was determined, as ml g^{-1}, being the minimum necessary to obtain a handleable plastic paste.

2.3. Measurement of setting time (ST), compressive strength (CS) testing and microstructure analysis

The fresh-cement pastes, β-TCP/MCPM and β-TCP/MCPM/Si, were put into a cylindrical mold (10 mm diameter × 5 mm height), and then immersed in simulated body fluid (SBF) solution at 37 °C, until reaching the *f*-ST. This solution contains ionic concentration similar to that of human blood plasma, and was prepared in accordance with previous protocols described by Kokubo and Takadama [31]. The hardening time of the cement was measured according to the Vicat method, based on the American Society for Testing and Materials C187-11 (ASTM). The ST was taken as the time wherein the paste hardened to such an extent that a needle (400 g, Φ = 1 mm) would not penetrate deeper than 0.5 mm into the sample or caused only imperceptible prints on its surface. At least five specimens were tested for obtaining the ST values.

Table 1. Composition of cement, liquid component, percentage of silica, L/P ratio and final setting time (*f*-ST).

Cement	SBA-15 (wt%)	Liquid	L/P ratio	*f*-ST (min)
βTCP-MCPM	—	PEG 400/H_2O	0.33	26
βTCP-MCPM + mesoporous silica	5%	PEG 400/H_2O	0.40	30

The measurements were presented as mean ± standard deviation (mean ± SD).

The specimens for the CS testing were prepared by placing the fresh paste into a Teflon® mold (6 mm diameter × 12 mm height), and then immersing them in SBF solution and storing them in a humidor with 100% relative humidity at 37 °C. After 1 and 7 d incubation in SBF solution, the samples were immediately removed from the molds. Then, the CS was measured at a loading rate of 1 mm min^{-1} using a Mechanical Testing Machine Instron 4443, according to ASTM F451. For each cement and soaking time, at least six replicates were tested. The measurements were presented as mean ± SD.

The apparent density and porosity of the samples were evaluated by the Archimedes' principle according to ASTM C20-00. Six specimens were immersed in deionized water for a period of 4 h for the immersed and wet mass measurements. The dry mass was determined after drying them for a period of 24 h in an oven at 100 °C. Subsequently, the apparent density and porosity were calculated using the following equations, respectively, where m_1 is the weight of the dry sample, m_2 is the weight of the submerged sample, m_3 is the weight of the wet sample and ρH_2O is the density of the water.

$$\rho = \left(\frac{m_1}{m_3 - m_2}\right) \times \rho H_2O \quad (1)$$

$$P = \left(\frac{m_3 - m_1}{m_3 - m_2}\right) \times \rho H_2O. \quad (2)$$

The results from the CS testing, apparent density and porosity were analyzed with one-way analysis of variance (ANOVA) followed by Tukey's test and the Student's *t*-test, respectively, where differences were considered statistically significant when $p < 0.05$.

The samples from the CS testing were immersed in acetone, to stop the hydration, and kept in the oven at 60 °C, for drying of the samples. The cross-section of the samples was observed by scanning electron microscopy (SEM) using a TM-1000 Hitachi operating at a voltage of 16 kV. The diffractograms were obtained using a diffractometer x-ray D8 Advance Bruker with a nickel filter and under Cu radiation (Kα) at 40 kV and 30 mA, with an angular scan from 10°–70° with step 0.02 s (2θ) and acquisition time of 3 s for each sample. The sample was ground into a fine powder using a ball mill for XRD analysis. The crystalline phases of the samples were determined by the standard crystallographic database records of the International Centre for Diffraction Data, Powder Diffraction File-2 (ICDD, PDF-2).

2.4. Injectability

The injectability of the cement formulations, β-TCP/MCPM and β-TCP/MCPM/Si, was evaluated by extrusion (i.e. quantification of residual-cement mass retained in the syringe after applying a standard force), during a predetermined injection time period. Syringes of 5 ml (BD Plastipak™) with an opening nozzle 2 mm in diameter were filled with 2.0 g fresh-cement paste. The syringe was placed between the compression plates of a Mechanical Testing Machine Instron 4443. After predetermined mixing times, the cement was extruded at a compression rate of 15 mm min^{-1} up to a maximum force of 100 N [32]. The injectability was calculated as: $I = [(m_i - m_e)/m_i] \times 100\%$, where I is the injectability, m_i is the initial mass and m_e is the end mass of the extrusion. All experiments were performed three times per sample, and the measurements were presented as mean ± SD.

2.5. *In vitro* bioactivity and degradability in SBF solution

For the evaluation of *in vitro* bioactivity and degradability, the fresh pastes were placed in a mold (15 mm diameter × 2.4 mm height). The demolded samples were soaked in SBF solution (surface area/volume ratio of 0.1 cm^{-1}) at 37 °C for 7 and 14 d before the bioactivity analysis, or up to 28 d before the degradability analysis [31]. The SBF solution was renewed every day [29]. After the respective immersion times, the samples were rinsed in deionized water and dried at room temperature (bioactivity analysis) or at 60 °C for 24 h (degradability analysis). For *in vitro* bioactivity analysis, the surface of the samples was covered with silver and analyzed by SEM using an S-4700 Hitachi microscope with a resolution of 1.5 nm, with variation in acceleration voltage of 0.5–30 kV, coupled to energy dispersive spectroscopy (EDS) Noran and System Six software. In addition, the changes in concentrations of calcium, phosphate and silicon ions in the SBF solution were analyzed by mass spectrometry inductively coupled plasma in an IRIS Advantage Thermo Jarrel Ash spectrometer, with a dual display system, a radio frequency source 40, 68 MHz, network Echelle type diffraction and charge injection device (CID) solid-state detector.

The degradation was calculated by the equation: $D = [(M_i - M_d)/M_i] \times 100\%$, where D is the degradation rate, M_i and M_d are dry weight of the initial specimen and the degraded specimen, respectively. The

values represent the average of three tests for each sample. All measurements were performed three times per sample, the values were presented as mean ± SD and analyzed with the Student's *t*-test, where differences were considered statistically significant when $p < 0.05$.

2.6. *In vitro* toxicity assays

2.6.1. Preparation of cement extracts

The injectable cements, β-TCP/MCPM and β-TCP/MCPM/Si, were prepared using 2 g of cement powder as described in section 2.1, previously sterilized by gamma radiation (15 Gky). The fresh paste was injected into a polypropylene tube. For *in vitro* assays, the extracts were prepared in accordance with ISO 10993-12:2008. Therefore, 10 ml 1:1 Ham-F10 + DMEM medium (Sigma®, St. Louis, MO) without fetal bovine serum (FBS) were added to the tubes containing the cements, and the tubes were incubated at 37 °C in an orbital shaker at 130 rpm. After the extraction, the conditioned medium was filtered with a syringe filter (0.22 μm). Four different concentrations of the extracts were used: C1 (200 mg ml^{-1}), C2 (20 mg ml^{-1}), C3 (2 mg ml^{-1}), C4 (200 μg ml^{-1}).

2.6.2. CHO-K1 cell culture

Chinese hamster ovary cells (CHO-K1) were cultured in 1:1 Ham-F10 + DMEM medium (Sigma®, St. Louis, MO) supplemented with 10% South America-sourced FBS (Gibco, Invitrogen) and 1% antibiotic antimycotic stabilized solution (Sigma®), 1% kanamycin (Gibco, Carlsbad, CA) in 25 cm^2 culture flasks at 37 °C in a humidified atmosphere with 5% CO_2. Cells were used among the third and eighth passages.

2.6.3. Cytotoxicity tests

2.6.3.1. XTT assay

CHO-K1 (2×10^4 cells) were seeded in 24-well plates in culture medium (1 ml, HAM-F10:DMEM; 1:1) supplemented with 10% FBS at 37 °C in a humidified atmosphere with 5% CO_2. After 24 h, the cells were washed with phosphate buffered saline (PBS) solution, and then treated with the respective cement extracts for 24 h. Each well was supplemented with 10% FBS. The negative control (NC) was cells with culture medium supplemented with 10% FBS without any treatment (untreated controls). For positive control (PC), the cells were treated with doxorubicin (3 μg ml^{-1}) for 24 h. After treatment, the cultures were washed with PBS solution and immediately 500 μl of DMEM without phenol red were added, followed by the addition of 60 μl of the XTT/electron solution (Cell Proliferation Kit II—Roche Applied Science). After 3 h reaction, the supernatant was transferred to a 96-well culture plate, and then the absorbance was measured using a microplate reader (VersaMax, Molecular Devices, Sunnyvale, CA) at 492 and 690 nm. Three independent experiments were conducted.

2.6.3.2. Clonogenic assay

CHO-K1 (5×10^4 cells) were seeded in 24-well plates in culture medium (1 ml, HAM-F10:DMEM; 1:1) supplemented with 10% of FBS at 37 °C, in 5% CO_2. After 24 h, the cells were washed with PBS solution, and then treated with the cement extracts supplemented with 10% FBS for 24 h. After treatment, exponentially growing cells were seeded at the number of 150 cells per 25 cm^2 flasks, in duplicate for each treatment. The flasks were incubated at 37 °C, in 5% CO_2, for 7 d without medium exchange. The colonies that formed were fixed with methanol:acetic acid:water (1:1:8 v/v/v) and stained with 5% Giemsa. The colonies were counted, and the cell-surviving fraction was calculated as the percent colonies in treated flasks relative to untreated controls (NC). Three independent experiments were conducted.

2.6.4. Genotoxicity evaluation: comet assay

The alkaline version of the comet assay was used in accordance with the method described by Singh *et al* (1988). CHO-K1 (27×10^3 cells) were seeded in 24-well plates in culture medium (1 ml, HAM-F10:DMEM; 1:1) supplemented with 10% FBS at 37 °C, in 5% CO_2. After 24 h, the cells were treated with the respective cement extracts supplemented with 10% FBS for 24 h. NC were cells with culture medium supplemented with 10% FBS without any treatment, while PC were the cells treated with hydrogen peroxide (80 μmol L^{-1} for 5 min). After treatment, 500 μl of trypsin was added to each well to detach the cells and was then transferred to a microtube. After centrifugation, the pellet was resuspended in 200 μl of 0.5% (w/v) low melting point agarose and the mixture was spread onto two microscope slides (Knittel, Germany) pre-coated with 1.5% (w/v) normal melting point agarose (Gibco). The slides were immersed in cold (4 °C) lysis solution (1% Triton X-100, 10% DMSO, 2.5 mmol L^{-1} NaCl, 100 mmol L^{-1} Na_2EDTA, 100 mmol L^{-1} Tris, pH 10) for 24 h. Immediately after this step, slides were placed in a horizontal electrophoresis cube containing freshly prepared electrophoresis buffer (1 mmol.L^{-1} Na_2EDTA, 300 mmol.L^{-1} NaOH, pH > 13) for at least 20 minutes for the DNA unwinding, and subsequently electrophoresis was performed at 43 V, 308 mA for 25 minutes. Afterwards, the slides were gently immersed in neutralizing buffer (0.4 mol L^{-1} Tris–HCl, pH 7.5) for 15 min and then fixed with ethanol. Three independent experiments were conducted.

The slides were stained with 0.2 mol L^{-1} ethidium bromide, and screened with a fluorescent microscope (DMLB—Leica) equipped with an excitation filter of 516–560 nm, a barrier filter of 590 nm and a 40 × objective. DNA damage was determined in a blind test in 100 nucleoids per slide. The level of DNA

damage was assessed by an image analysis system (Tri-Tek CometScore® 1.5, 2006, Sumerduck, VA, USA), and the DNA percentage in the tail and tail moment were obtained for each treatment. A visual score was also used to compute DNA damage from the comets. Five classes were used, from 0 (no tail) to 4 (almost all DNA in tail) [33] and the DNA damage index (DDI) was calculated.

2.6.5. Mutagenicity evaluation: cytokinesis-blocked micronucleus (CBMN) assay

CBMN assay was performed according to Fenech [34]. CHO-K1 cells (37×10^4 cells) were seeded in 25 cm^2 culture flasks at 37 °C, in 5% CO_2. After 24 h of seeding, cells were exposed for 24 h to the cement extracts supplemented with 10% FBS. The NCs were culture flasks with culture medium supplemented with 10% FBS, while PCs were treated with doxorubicin (0.15 $\mu g.ml^{-1}$) for 4 h. Cytochalasin-B (CytB) (1 mg ml^{-1}) was added to the CHO-K1 cultures and left for 24 h. After treatment, the cultures were washed with PBS solution, trypsinized and centrifuged for 7 min at 400 $\times g$. The pellet was resuspended in cold hypotonic solution (0.3% KCl w/v) for 5 min. This cell suspension was centrifuged again and resuspended in 3 ml of methanol: acetic acid (3:1) solution and 200 μl 1% formalin. After centrifugation, the cell suspensions were carefully dropped onto a slide with a film of distilled water at 4 °C. The slides were stained with 5% Giemsa solution diluted in phosphate buffer (Na_2HPO_4 0.06 mol L^{-1}, KH_2PO_4 0.06 mol L^{-1}—pH 6.8) for 7 min, then rinsed in distilled water, and dried at room temperature. Three independent experiments were conducted.

Five hundred viable cells were scored to determine the frequency of cells from 1–4 nuclei and we calculated the nuclear division index (NDI) using the formula: [NDI = M1 + 2(M2) + 3(M3) + 4 (M4)/N], where *M*1–*M*4 represents the number of cells with 1–4 nuclei, respectively, and *N* is the total number of viable cells [35]. The frequency of binucleated cells with micronuclei (FBNC-MN) and the total frequency of micronuclei (FMN) were scored in 1,000 binucleated cells [34, 36]. Moreover, the frequency of nucleoplasmic bridges and nuclear buds was analyzed.

2.6.6. Statistical analysis

The results from *in vitro* assays were submitted to the Kolmogorov–Smirnov test, which was used for testing normality. The data presented adherence to the normal curve, and ANOVA followed by Tukey's test were applied to the data. Graphpad Prism version 5.01 software was used to perform the tests. Differences were considered statistically significant when $p < 0.05$.

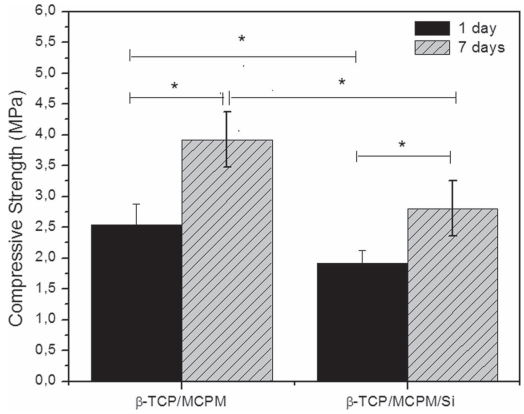

Figure 2. Compressive strength of the β-TCP/MCPM and β-TCP/MCPM/Si cements immersed in SBF solution after 1 and 7 d. (*) $p < 0.05$ (Tukey's test).

3. Results

3.1. Characterization of the cements

3.1.1. ST, compression strength and microstructure analysis

The *f*-ST obtained by the β-TCP/MCPM and β-TCP/MCPM/Si cements, respectively, are shown in table 1. The cements synthetized in this study showed that the L/P ratio allowed *f*-ST values close to 25 and 30 min for β-TCP/MCPM and β-TCP/MCPM/Si, respectively, under conditions to simulate the setting *in situ*.

The compressive strength data are shown in figure 2. The β-TCP/MCPM cement obtained 2.54 ± 0.33 MPa and β-TCP/MCPM/Si 1.95 ± 0.20 MPa, after immersion in SBF solution for 24 h. The data showed that the compressive strength of both cements increased according to the immersion time. At 7 d, the values measured were 3.95 ± 0.44 MPa and 2.81 ± 0.45 MPa, respectively. These results suggest that aqueous-medium diffusion inside the cement is continuous and promotes the hydration of the cement and the increase of the DCPD content, which leads to the increase of its mechanical properties [37].

Figure 3 shows the mean values of porosity and apparent density of the β-TCP/MCPM and β-TCP/MCPM/Si cements. The values measured of the apparent porosity of the β-TCP/MCPM and β-TCP/MCPM/Si cements were 37% and 42%, respectively. Moreover, there is an inverse relationship between density and porosity, whereas lower porosity percentage presented higher density value. However, no significant difference was measured for both density and apparent porosity values.

Figure 4 shows the XRD patterns of β-TCP/MCPM and β-TCP/MCPM/Si cements after immersion in SBF solution for 1 d, compared with the initial β-TCP powder. The β-TCP/MCPM cement setting resulted in a mixture of monetite with diffraction peaks at $2\theta = 26.5°$, 30.1° and 32.8° (JCPDS #00-009-0080)

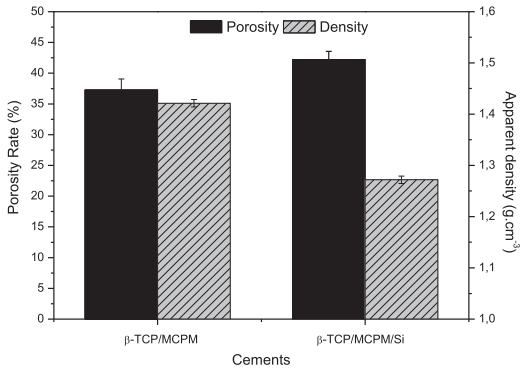

Figure 3. Density and apparent porosity of the β-TCP/MCPM and β-TCP/MCPM/Si cements. No significant difference was measured between these cements (Student's t-test).

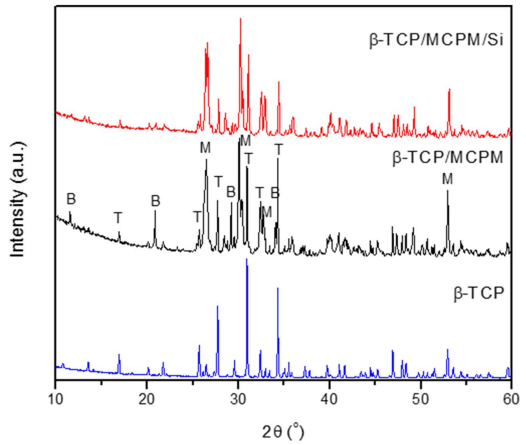

Figure 4. XRD patterns of the β-TCP powder compared with the β-TCP/MCPM and β-TCP/MCPM/Si cements in SBF solution after 1 d; B = brushite, M = monetite, T = β – TCP.

and β-TCP at $2\theta = 27.7°$, 30.9° and 34.5° (JCPDS #00-009-0169) in most proportions. The characteristic peaks observed at $2\theta = 11.5°$, 20.8° and 29.4° were however attributed to a minority brushite phase (JCPDS #00-009-0077). The characteristic peaks related to brushite were not observed in the XRD pattern of the β-TCP/MCPM/Si cement.

Figure 5 shows SEM images of the fracture surface of the β-TCP/MCPM and β-TCP/MCPM/Si cements. The micrographs revealed different crystalline phases for both cements and large crystals in lamellar-form can be attributed to the brushite and monetite phase, and small particles to the unreacted β-TCP [37]. This heterogeneous morphology of the crystals can also be related to the use of PEG as the liquid component to obtain calcium phosphate pastes. The exchange of non-aqueous liquid and aqueous solution is relatively slow during the setting process and can form different components [8], as confirmed by XRD analysis (figure 4).

3.1.1.1. Injectability

Figure 6 shows the results obtained for the β-TCP/MCPM and β-TCP/MCPM/Si cements. The incorporation of the mesoporous silica (5 wt%) into the cement increased the paste-injectability time compared with the β-TCP/MCPM cement. The final injectability to the β-TCP/MCPM cement was 15 min and was not able to be extruded (0% extruded paste) whereas the β-TCP/MCPM/Si cement at 15 min after handling contained around 50% of the material to be extruded for a 100 N force.

3.1.1.2. In vitro *bioactivity and degradability in SBF solution*

SEM images of the cements after immersion in SBF solution are shown in figures 7 and 8. After 7 d, the surfaces of both cements revealed similar morphology to crystals in the form of needles (figures 7(a) and 8(a)). At 14 d, surface micrographs showed that the amount of crystals on both cement surfaces increased with the immersion time, promoting the precipitation of a uniform crystalline layer (figures 7(b) and 8(b)). The EDS spectrum (figure 8(c)) showed that the presence of mesoporous silica in the β-TCP/MCPM/Si cement could not be detected on the surface after 14 d of immersion. This result may be related to the homogeneous precipitation or secondary nucleation of apatite crystals. SEM images showed the precipitation/nucleation apatite on the cement surfaces with the formation of needle-like crystals in the initial stages and globular formations, and the amount and size of the crystals grew according to the immersion time. These findings indicate that both cements, β-TCP/MCPM and β-TCP/MCPM/Si, demonstrated excellent bioactivity. However, the β-TCP/MCPM/Si cement promoted the formation of a more homogeneous layer.

The degradation rate for both cements was characterized by mass loss after immersion of the cements in SBF solution (figure 9). The degradation rate for both cements was higher at the first 7 d (figure 9(a)) in agreement with processes controlled by a diffusion mechanism, showing a similar profile to the increase P (for both cements) and Si ions (β-TCP/MCPM/Si cement) (figure 10). In addition, the pH values in the SBF solution at 37 °C was reduced from 7.4 to 6.0 at the first 7 d (figure 9(b)), which can be attributed to the hydration reaction of DCPD cements. After 7 d, the degradation rate decreased and the pH values were gradually increased and remained constant around 7.5 (figure 9(b)). The β-TCP/MCPM/Si cement showed a higher percentage of degradation (32%) than the β-TCP/MCPM cement (24%) (figure 9(a)), suggesting that the presence of the mesoporous silica may be associated with a higher dissolution rate, which can be attributed to the higher porosity of *the* β-TCP/MCPM/Si cement as the higher solubility of these particles [29].

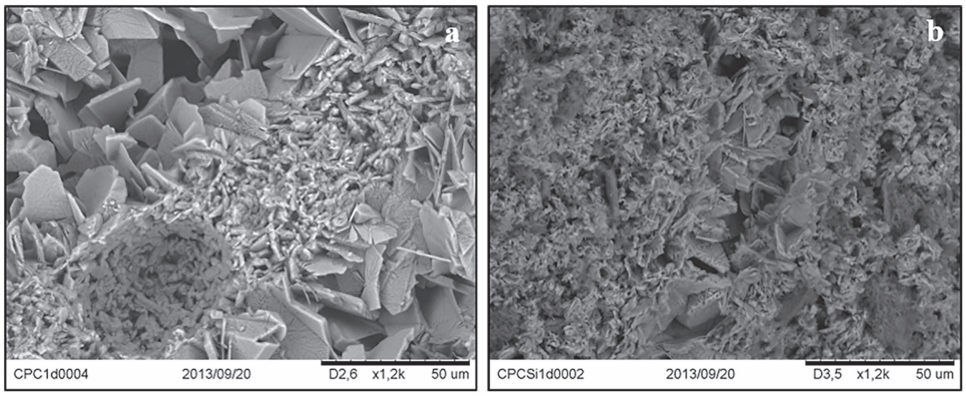

Figure 5. SEM images of the fracture surface of the β-TCP/MCPM (a) and β-TCP/MCPM/Si (b) cements soaking in SBF solution after 1 d (1200×).

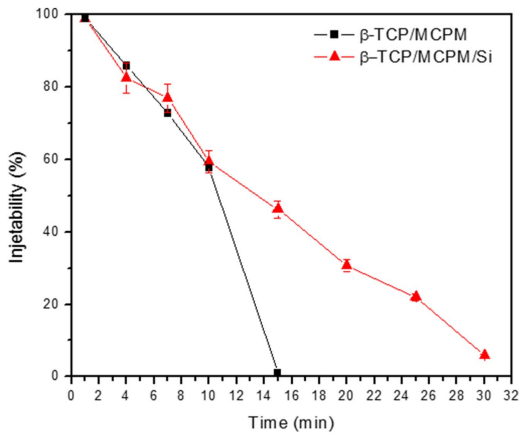

Figure 6. Injectability of the β-TCP/MCPM and β-TCP/MCPM/Si cements versus time after the start of handling.

The Ca, P and Si amount in the SBF solution after different periods of interaction with the β-TCP/MCPM and β-TCP/MCPM/Si cements is shown in figure 10. It is interesting to note that the Ca concentration constantly decreased, while the P concentration increased in the early stages. These findings could be explained by the dissolved Ca in the SBF solution being incorporated into the precipitated apatite. Considering that, the Ca/P molar ratio is higher to HA than to brushite, whereas each mole of dissolved brushite is released a P extra amount to the nucleation of the HA. The Si concentration steadily increased in a range of the lowest values according with degradation process in figure 9.

3.2. CHO-K1 cells *in vitro* toxicity results

Figure 11(a) shows the mean and standard error (mean ± SE) for cell viability obtained by XTT assay for the β-TCP/MCPM and β-TCP/MCPM/Si cements. Cell viability is related to the measuring absorbance and the NC was considered as 100% cell viability. The β-TCP/MCPM and β-TCP/MCPM/Si cements' original extracts (C1 concentration = 200 mg ml^{-1}) revealed mild cytotoxic effects compared with the NC ($p < 0.05$), although the β-TCP/MCPM/Si cement has demonstrated cell viability to C1 concentration higher than 60%. For the cells that were treated with the less concentrated extracts (C2, C3 and C4), no cytotoxic effects were observed ($p < 0.05$) (figure 11(a)) in the β-TCP/MCPM/Si cement.

Figure 11(b) shows the surviving fraction obtained by the clonogenic cell survival assay of the β-TCP/MCPM and β-TCP/MCPM/Si cements. This assay measures the proliferative ability of single cells to form a colony and is routinely used as a sensitive model for assessing long-term cytotoxicity [38]. Considering the XTT results, CHO-K1 cells treated with C1 and C2 exhibited a proliferation rate lower than the NC. However, no statistical differences were observed in the clonogenic assays. The results suggest that even C1- β-TCP/MCPM/Si and C1 and C2- β-TCP/MCPM extract cements showed cytotoxicity to CHO-K1 cells by the XTT assay (figure 11(a)). However, it did not significantly compromise cells treated with conditioned media that maintained their proliferative ability.

The potential genotoxic effect of the β-TCP/MCPM/Si cement was evaluated by comet assay and the results are shown in figure 12. The electrophoresis in alkaline conditions is the most comprehensive version of this test and was used to verify whether the β-TCP/MCPM/Si cement would be able to promote a genotoxic behavior in CHO-K1 cells. These results showed that the β-TCP/MCPM/Si cement did not show damage level in any treatment compared with the NC in any of the examined parameters ($p < 0.05$). The results showed DDI was between 0 and 0.5, which corresponds to less than 5% of DNA damage [39].

The mutagenicity was evaluated by the micronucleus testing with the β-TCP/MCPM/Si cement. The results are summarized in table 2. The results showed statistically significant difference of the FBMN and FMN values between the NC and C1, as well as the presence of nucleoplasmatic bridges.

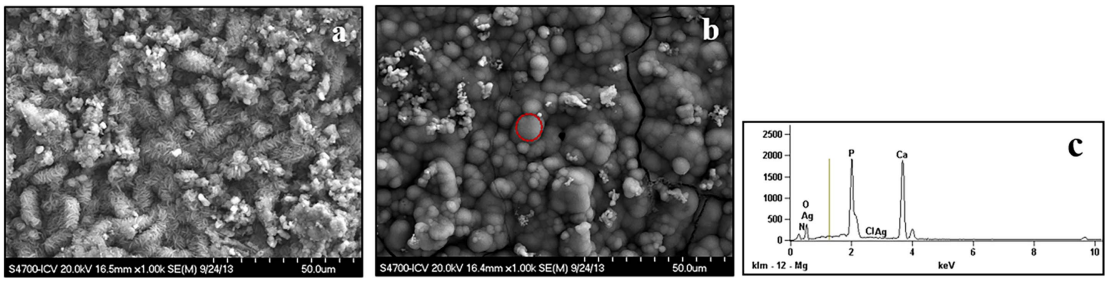

Figure 7. β-TCP/MCPM surface SEM images after immersion in SBF solution at 7 d (a) and 14 d(b). EDS patterns after 14 d (c).

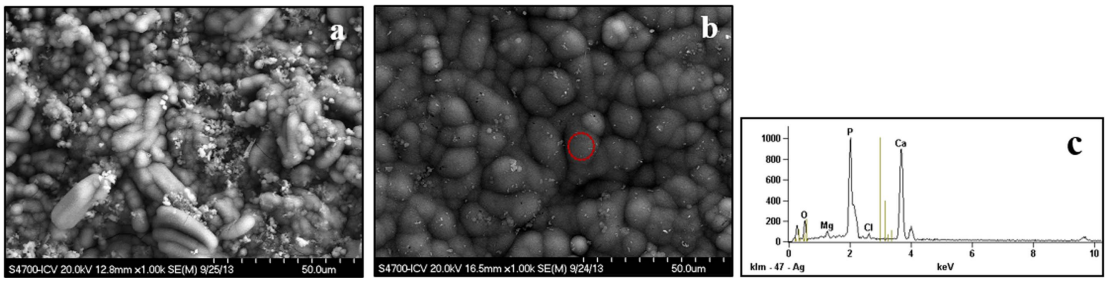

Figure 8. β-TCP/MCPM/Si surface SEM images after immersion in SBF solution at 7 d(a) and 14 d (b). EDS patterns after 14 d (c).

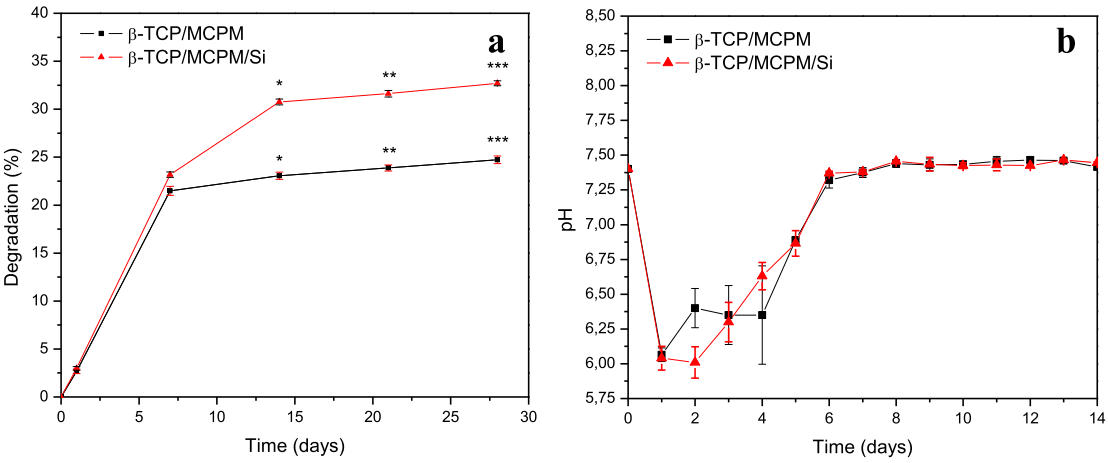

Figure 9. Degradation rate (a) and pH values (b) of the β-TCP/MCPM and β-TCP/MCPM/Si cements. (*) 14, (**) 21 and (***) 28 d results $p < 0.05$ (Student's t-test).

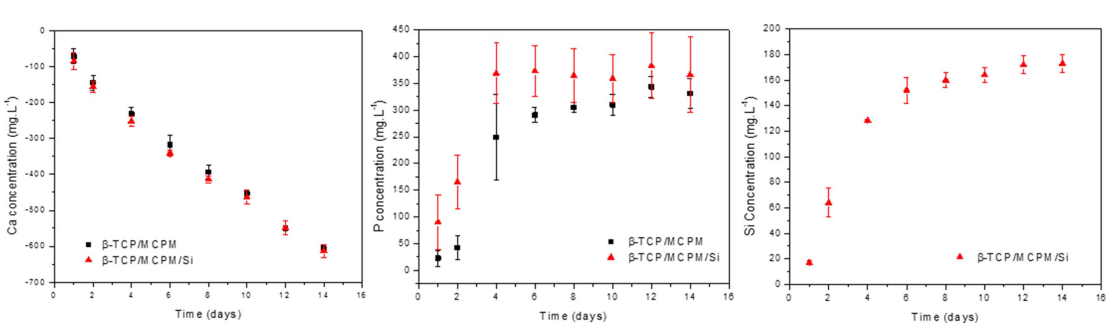

Figure 10. Chemical analysis of the SBF solutions after the reaction with the β-TCP/MCPM and β-TCP/MCPM/Si cements for different times.

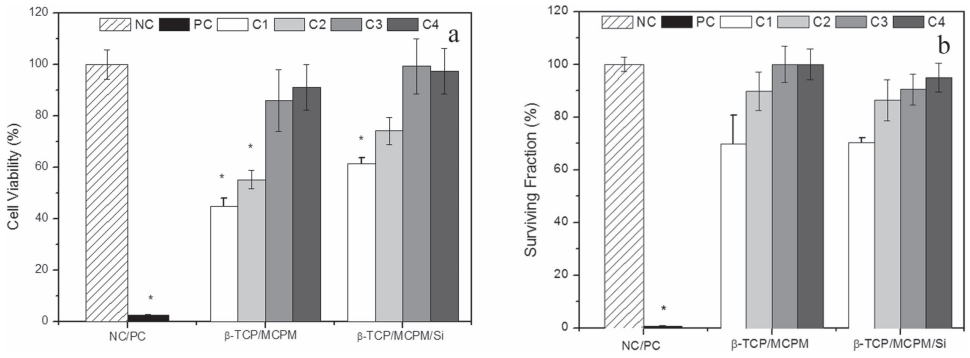

Figure 11. XTT assay (a) and clonogenic survival (b) for the β-TCP/MCPM and β-TCP/MCPM/Si cements. (*) Indicates a statistically significant difference compared with the NC. Data are reported as mean $\pm$ SE ($p < 0.05$, Tukey's test).

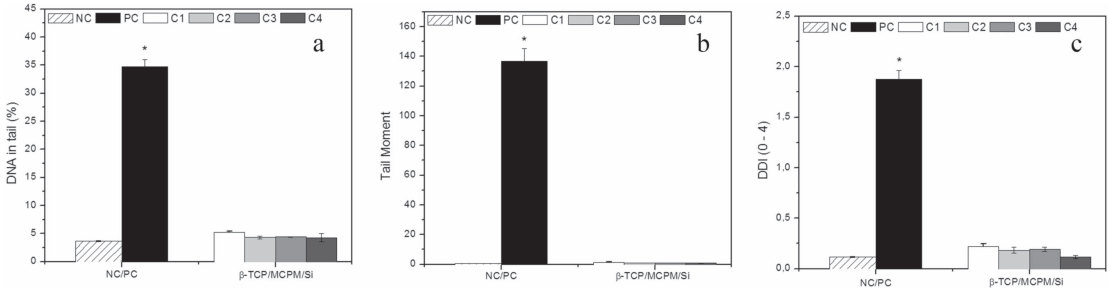

Figure 12. β-TCP/MCPM/Si cement comet assay; (a) average percentage of DNA found on the tail of nucleoids; (b) tail moment; (c) DDI. Data are reported as mean $\pm$ SE; (*) $p < 0.05$ compared with the NC (Tukey's test).

Table 2. NDI, FBC-MN and FMN, nucleoplasmic bridges and nuclear blebs obtained for the β-TCP/MCPM/Si cement extracts. Data are reported as mean $\pm$ SE; (*) $p < 0.05$ compared with the NC (Tukey's test).

Samples	NDI	FBC-MN	FMN	N. Bridges	N. Blebs
NC	1.9 $\pm$ 0.01	9.2 $\pm$ 0.42	9.2 $\pm$ 0.42	16.0 $\pm$ 1.10	10.0 $\pm$ 1.03
PC	1.6 $\pm$ 0.01*	90.0 $\pm$ 3.14*	154.0 $\pm$ 2.81*	54.0 $\pm$ 1.46*	98.0 $\pm$ 2.10*
β-TCP/MCPM/Si-C1	1.1 $\pm$ 0.02	26.0 $\pm$ 1.42*	33.0 $\pm$ 1.46*	20.2 $\pm$ 0.12*	17.0 $\pm$ 1.43
β-TCP/MCPM/Si-C2	1.9 $\pm$ 0.01	12.0 $\pm$ 1.70	12.0 $\pm$ 1.70	10.0 $\pm$ 1.12	2.0 $\pm$ 0.26
β-TCP/MCPM/Si-C3	1.9 $\pm$ 0.05	11.3 $\pm$ 0.51	11.3 $\pm$ 0.51	3.6 $\pm$ 0.35	4.0 $\pm$ 1.02
β-TCP/MCPM/Si-C4	2.1 $\pm$ 0.01	4.2 $\pm$ 0.86	4.2 $\pm$ 0.86	5.9 $\pm$ 0.86	2.2 $\pm$ 0.46

4. Discussion

The mixture of MCPM and β-TCP powders in the presence of water reacts and forms a product known as brushite (DCPD), according to the following reaction [7, 40]:

$$Ca_3(PO_4)_2 + Ca(H_2PO_4)_2.H_2O + 7H_2O \rightarrow 4CaHPO_4.2H_2O. \quad (4)$$

Of this reaction, the major product of hydration is expected to be brushite, besides a fraction of unreacted β-TCP and a non-hydrated brushite phase, known as monetite (DCPA, $CaHPO_4$), when the mixture is prepared with excess β-TCP. The results showed monetite as the main product of hydration with a significant fraction of unreacted β-TCP. Monetite was also found in samples aged at 37 °C in PBS in DCPD cements based on β-TCP/MCPM and aqueous solution [41].

The setting of the β-TCP/MCPM and β-TCP/MCPM/Si cements depended on the balance between PEG and the aqueous solution. As a viscous material, PEG can improve the cohesion and the rheological property of calcium phosphate cements, but at the same time prevents the curing reaction due to the polymeric coating of the solid cement particles [8]. It was noted that this exchange is relatively slow and promotes the formation of two crystalline compounds, monetite and brushite, and the remaining β-TCP particles of solid precursor material, as confirmed by XRD. In accordance with these results, it is suggested that the period of 1 d was not sufficient for complete

hydration of the cements, especially for the β-TCP/MCPM/Si cement, wherein the presence of silica may have delayed hydration [42].

Clinical approaches for applications of injectable bone materials are based on suitable handling time, in which the cement should be applied by extrusion before the hardening process, and the *f*-ST should preferably be close to 20 min [43]. The *f*-ST is known as the time required for cement paste to stiffen to a defined consistency, i.e. when the paste completely loses its plasticity [44]. It is known that the L/P ratio directly influences the *f*-ST and mechanical resistance. In this work, the L/P ratios were chosen to produce pastes of workable consistency. Therefore, the results corroborated to the data previously obtained by Han *et al* [8] to βTCP-MCPM cements using PEG as a liquid component and similar L/P ratios, showing that *f*-ST decreased as the L/P ratio decreased. In general, the β-TCP/MCPM cements, when mixed with water, showed a relatively rapid setting and the cements studied demonstrate an advantage by allowing more time for the operations, because the paste only sets *in situ*.

However, the compressive strength data decreased with the increase of the liquid component, because the porosity percentage is directly proportional to the L/P ratio [45] and the voids tend to negatively influence the mechanical resistance. In addition, the presence of the remaining β-TCP may induce a negative effect on the mechanical properties of the cements due to the pores existing between the crystals, and there may not be enough crystalline phases to bind the particles of the cement after hardening [45]. A standard procedure for reducing the porosity is to decrease the L/P ratio, whereas the curing time of a moldable and injectable paste determines a limit of this ratio. Indeed the premixing of the mesoporous silica particles with the cement solid components showed an increase in the L/P ratio to obtain a moldable paste containing a similar ST to the silica-free cement. Therefore, these cements presented higher porosity and lower values of mechanical property than silica-free cement.

On the other hand, open porosity is a favorable factor for osteoconductive property, which depends on the pore size and allows the bone neoformation inside of the material [46]. Thus, the cements synthesized in this study tend to favor this behavior. In addition, this value is not stable and can be altered by increasing the immersion time and interaction of the cements with the physiological medium; thereby increasing the porosity of the cement due to its degradation and/or HA precipitation/nucleation on its surface.

Bioactive glasses are able to form apatite crystals on their surface, after an immersion period in SBF solution [47–49]. The addition of the mesoporous silica in the cement, β-TCP/MCPM/Si, could allow the formation of a hydrated silica layer, which provides favorable sites for the nucleation of apatite crystals. Considering that apatite formation on the material surface depends on the supersaturated body fluid containing Ca^{2+} and PO_4^{3-} íons, the nucleation site of the apatite is formed on a material inside the body, followed by continuous and spontaneous growth by adsorption of these ions present in the body fluid [50]. However, the deposition/precipitation process acts at a low rate, which results in the absence of the formation of a homogeneous layer of apatite in the early stages of implantation [51].

The globular morphology observed in SEM images is related to the presence and precipitation of carbonated apatite (CA) or calcium-deficient hydroxyapatite (CDHA) [52, 53]. The concentration of carbonate ions (CO_3^{2-}) in the apatite molecule defines its morphology, which may vary from globular to acicular crystals [54], considering that CO_3^{2-} ions can substitute in the apatite structure for either or both OH and PO_4^{3-}PO43- groups, referred to as type A or type B substitutions, respectively. Apatite with type B substitution (type B carbonate apatite) has demonstrated to be more similar to the carbonate substitution in biologic apatite [55]. In addition, in this carbonate apatite the increase in carbonate content is directly associated with the substitution of Ca^{2+} by Na^{+} ions, which allows morphological changes in apatite crystals from acicular to rods/globular crystals [55].

The degradation rate is primarily governed both by chemical composition and physical characteristics of the respective material. On the other hand, the degradation rate for biomaterials with therapeutic approaches for bone filling should be concomitant to bone neoformation [56]. Therefore, the degradability in physiological media is one of the most important features to be evaluated in materials for application in bone repair. In addition, brushite is metastable under physiological conditions [57], and for this reason brushite cements degrade much faster than apatite ones [5, 8]. Furthermore, the results showed that the dissolution rate can be changed with the incorporation of seed materials in the cement solid component, and the L/P ratio, being in this study the presence of mesoporous silica, which increases the degradation process.

Mechanical injections of cement were performed in order to evaluate the key time for suitable handling and injectability of the cements. The injectability property of a paste/cement is very important when the materials are used in applications for bone defects, because of limited accessibility and the use of this material for minimally invasive surgical techniques. According to Khairoun *et al* [58], poor injectability is characterized by phase separation between the solid and liquid components, resulting in a partial extrusion. The results showed that even with different injectability times, this behavior was not observed in any of the cements analyzed (maximum load for injection 100 N). Therefore, the best injectability property is when a large amount of cement is extruded from the syringe in a shorter ST and this property is directly

related to cement viscosity. Therefore, for a cement to be injectable, the paste must have low viscosity and offer little resistance to flow from the syringe. The β-TCP/MCPM cement was less injectable than the β-TCP/MCPM/Si cement and this result could be related to the presence of silica particles [29, 42].

When there is excess β-TCP, the degradation of β-TCP-MCPM cement in deionized water promotes a decrease of pH value to moderately acid, and then a balance between DCPD crystals and the remaining β-TCP determines the final pH value [41]. Furthermore, the cement pH exerts a strong influence on the cytotoxicity test and it is the principal controlling factor of the Ca and P concentrations [59]. Moreover, endoplasmatic reticulum stress caused by an excess of Ca^{2+} ions may lead to apoptosis [60]. Thus, the decrease of the pH, due to hydration (figure 9(b)), could promote a cytotoxic effect as shown by C1 extracts.

The comet assay is widely used to assess DNA damage by alkylating agents, intercalating and oxidizing the nuclei acid. Gulum *et al* [61] indicated that decreased antioxidant capacity and increased oxidative stress might be associated with increased DNA damage. Altay *et al* [62] have evaluated the genotoxic potential of three concentrations of extracts of Cimentek® in mononuclear leukocytes and observed that there was DNA damage (even without cytotoxicity), which was positively correlated with increasing cement concentration in culture medium. On the other hand, there was no significant correlation between DNA damage and oxidative status parameters. It was also observed that CPC extract concentrations of $\geqslant 100\ \mu g\ ml^{-1}$ induce DNA damage [63]. The results of this study showed that no β-TCP/MCPM/Si cement extract was significantly different from the NC. Therefore, it was not genotoxic to CHO-K1 cells.

The MN assay was carried out with blocking cytokinesis in order to evaluate DNA damage and cell division [64]. Its importance may be related to the theory that its genesis and the MN would look like, and any chromosomal fragment that can stay in the cytoplasm during cell division would be encapsulated forming a budding, that if it were to disconnect the core, it would take the form of an MN [65]. Chun *et al* [66] have evaluated the cytotoxic and genotoxic potential of Bio-CPC reinforced by chitosan and showed that the extracts in the same concentration as C3-β-TCP/MCPM/Si or less have cytotoxicity against the MDPC-23 mouse odontoblast-like cells after 24 h of incubation. However, the cytotoxic effect decreased with increasing incubation time. In contrast, they observed no change in FBMN when these cells were incubated in $100\ \mu g\ ml^{-1}$ extract, which was a concentration lower than C4-β-TCP/MCPM/Si. The same was observed in this study, where β-TCP/MCPM/Si extracts with concentration greater than $100\ \mu g\ ml^{-1}$ (as C2, C3 and C4) showed no statistically significant difference in the frequency of cells with MN. This indicated that under certain treatment conditions, exposure to the test agent did not result in a significant increase in chromosomal damage in the population of analyzed cells.

5. Conclusions

The β-TCP/MCPM and β-TCP/MCPM/Si cements were successfully synthesized. The characterization showed that the presence of mesoporous silica particles in the composition promoted better physicochemical properties compared with silica-free cement, such as *f*-ST, injectability, L/P ratio and porosity, but with lower mechanical property. The cements showed *in vitro* bioactivity immersed in the SBF solution by the precipitation of an apatite layer on its surface. With regard to the toxicity assays, the β-TCP/MCPM and β-TCP/MCPM/Si cements showed lower CHO-K1 cell viability after treatment with more concentrated extracts, which can be related to changes in pH. Indeed, the reproductive capacity was not compromised by this behavior. Considering the mutagenicity and genotoxicity assays, lower extract concentrations of β-TCP/MCPM/Si cement did not promote significant DNA damage. Thus, the βTCP-MCPM cement associated with mesoporous silica might be considered as a potential bone substitute for the repair and regeneration of bone defects.

Acknowledgments

The authors gratefully acknowledge the financial support of the Brazilian research funding institutions FAPESP (# 2012/21735-6) and Capes-PDSE (# 0224-13-8), and Ministerio de Economía y Competitividad of Spain (MAT2013-48426-C2-1R).

ORCID iDs

L S Mendes https://orcid.org/0000-0001-5468-4397

References

[1] Saska S, Mendes L S, Minarelli A M M and Capote T S O 2015 Bone substitute materials in implant dentistry *Current Concepts in Dental Implantology* ed I Turkyilmaz (Rijeka: Intech)

[2] Tamimi F *et al* 2009 Minimally invasive maxillofacial vertical bone augmentation using brushite based cements *Biomaterials* **30** 208–16

[3] Liu W *et al* 2014 A novel injectable, cohesive and toughened Si-HPMC (silanized-hydroxypropyl methylcellulose) composite calcium phosphate cement for bone substitution *Acta Biomaterialia* **10** 3335–45

[4] Ginebra M P, Canal C, Espanol M, Pastorino D and Montufar E B 2012 Calcium phosphate cements as drug delivery materials *Adv. Drug. Deliv. Rev.* **64** 1090–110

[5] Apelt D *et al* 2004 *In vivo* behavior of three different injectable hydraulic calcium phosphate cements *Biomaterials* **25** 1439–51

[6] Bohner M, Merkle H P and Lemaître J 2000 *In vitro* aging of a calcium phosphate cement *J. Mater. Sci., Mater. Med.* **11** 155–62

[7] Mirtchi A A, Lemaître J and Hunting E 1989 Calcium-phosphate cements—action of setting regulators on the properties of the β-tricalcium phosphate monocalcium phosphate cements *Biomaterials* **10** 634–8

[8] Han B *et al* 2009 β-TCP/MCPM-based premixed calcium phosphate cements *Acta Biomaterialia* **5** 3165–77

[9] Legeros R Z, Chohayeb A and Shulman A 1982 Apatitic calcium phosphates: possible dental restorative materials *J. Dent. Res.* **61** 343–7

[10] Brown W E and Chow L C 1983 A new calcium-phosphate setting cement *J. Dent. Res.* **62** 672–6

[11] Welch R D, Zhang H and Bronson D G 2003 Experimental tibial plateau fractures augmented with calcium phosphate cement or autologous bone graft *J. Bone Joint. Surg.* **85A** 222–31

[12] Aral A, Yalcin S, Karabuda Z C, Anil A, Jansen J A and Mutlu Z 2008 Injectable calcium phosphate cement as a graft material for maxillary sinus augmentation: an experimental pilot study *Clin. Oral Implants Res.* **19** 612–7

[13] Libicher M *et al* 2006 Osseous integration of calcium phosphate in osteoporotic vertebral fractures after kyphoplasty: initial results from a clinical and experimental pilot study *Osteoporos. Int.* **17** 1208–15

[14] Ooms E M, Wolke J G C, van der Waerden J and Jansen J A 2003 Use of injectable calcium-phosphate cement for the fixation of titanium implants: an experimental study in goats *J. Biomed. Mater. Res.* B **66B** 447–56

[15] Takemasa R, Kiyasu K, Tani T and Inoue S 2007 Validity of calcium phosphate cement vertebroplasty for vertebral non-union after osteoporotic fracture with middle column involvement *Spine J.* **7** 148–55

[16] Alcaide M, Portoles P, Lopez-Noriega A, Arcos D, Vallet-Regi M and Portoles M T 2010 Interaction of an ordered mesoporous bioactive glass with osteoblasts, fibroblasts and lymphocytes, demonstrating its biocompatibility as a potential bone graft material *Acta Biomaterialia* **6** 892–9

[17] Manzano M *et al* 2011 Comparison of the osteoblastic activity conferred on Si-doped hydroxyapatite scaffolds by different osteostatin coatings *Acta Biomaterialia* **7** 3555–62

[18] Bharali D J *et al* 2005 Organically modified silica nanoparticles: a nonviral vector for *in vivo* gene delivery and expression in the brain *Proc. Natl Acad. Sci. USA* **102** 11539–44

[19] Kang K *et al* 2009 Preparation and characterization of chemically functionalized silica-coated magnetic nanoparticles as a DNA separator *J. Phys. Chem.* B **113** 536–43

[20] Lozano D *et al* 2010 Osteostatin-loaded bioceramics stimulate osteoblastic growth and differentiation *Acta Biomaterialia* **6** 797–803

[21] Luo Z Y *et al* 2015 Peptide-laden mesoporous silica nanoparticles with promoted bioactivity and osteo-differentiation ability for bone tissue engineering *Colloids Surf.* B **131** 73–82

[22] Hench L L, Splinter R J, Allen W C and Greenlee T K 1971 Bonding mechanisms at the interface of ceramic prosthetic materials *J. Biomed. Mater. Res.* **5** 117–41

[23] Pereira M M, Clark A E and Hench L L 1995 Effect of texture on the rate of hydroxyapatite formation on gel-silica surface *J. Am. Ceram. Soc.* **78** 2463–8

[24] Vallet-Regí M, Pérez-Pariente J, Izquierdo-Barba I and Salinas A J 2000 Compositional variations in the calcium phosphate layer growth on gel glasses soaked in a simulated body fluid *Chem. Mater.* **12** 3770–5

[25] Andersson J, Areva S, Spliethoff B and Linden M 2005 Sol–gel synthesis of a multifunctional, hierarchically porous silica/apatite composite *Biomaterials* **26** 6827–35

[26] Izquierdo-Barba I *et al* 2009 Influence of mesoporous structure type on the controlled delivery of drugs: release of ibuprofen from MCM-48, SBA-15 and functionalized SBA-15 *J. Sol-Gel Sci. Technol.* **50** 421–9

[27] Hench L L 2006 The story of bioglass (R) *J. Mater. Sci., Mater. Med.* **17** 967–78

[28] Wang X, Ye J, Wang Y and Chen L 2007 Self-setting properties of a β-dicalcium silicate reinforced calcium phosphate cement *J. Biomed. Mater. Res.* B **82B** 93–9

[29] Yu L *et al* 2013 A novel injectable calcium phosphate cement-bioactive glass composite for bone regeneration *Plos One* **8** 4

[30] Mendes L S, Saska S, Martines M A U and Marchetto R 2013 Nanostructured materials based on mesoporous silica and mesoporous silica/apatite as osteogenic growth peptide carriers *Mater. Sci. Eng.* C **33** 4427–34

[31] Kokubo T and Takadama H 2006 How useful is SBF in predicting *in vivo* bone bioactivity? *Biomaterials* **27** 2907–15

[32] Ginebra M P, Rilliard A, Fernández E, Elvira C, San Román J and Planell J A 2001 Mechanical and rheological improvement of a calcium phosphate cement by the addition of a polymeric drug *J. Biomed. Mater. Res.* **57** 113–8

[33] Collins A R 2004 The comet assay for DNA damage and repair *Mol. Biotechnol.* **26** 249–61

[34] Fenech M 2000 The *in vitro* micronucleus technique *Mutat. Res./Fund. Mol. Mech. Mutagen.* **455** 81–95

[35] Eastmond D A and Tucker J D 1989 Identification of aneuploidy-inducing agents using cytokinesis-blocked human-lymphocytes and an antikinetochore antibody *Environ. Mol. Mutagen.* **13** 34–43

[36] Tolbert P E, Shy C M and Allen J W 1992 Micronuclei and other nuclear anomalies in buccal smears: methods development *Mutat. Res.* **271** 69–77

[37] Barinov S M and Komlev V S 2016 Approaches to the fabrication of calcium phosphate-based porous materials for bone tissue regeneration *Inorg. Mater.* **52** 339–46

[38] Sumantran V N *et al* 2007 Differential growth inhibitory effects of W-somnifera root and E-officinalis fruits on CHO cells *Phytother. Res.* **21** 496–9

[39] Kobayashi H, Sugiyama C, Morikawa Y, Hayashi M and Sofuni T 1995 A comparison between manual microscopic analysis and computerized image analysis in the single cell gel electrophoresis assay *MMS Commun.* **3** 103–15

[40] Charriere E *et al* 2001 Mechanical characterization of brushite and hydroxyapatite cements *Biomaterials* **22** 2937–45

[41] Bohner M, van Landuyt P, Merkle H P and Lemaitre J 1997 Composition effects on the pH of a hydraulic calcium phosphate cement *J. Mater. Sci., Mater. Med.* **8** 675–81

[42] Huan Z G and Chang J 2009 Calcium-phosphate-silicate composite bone cement: self-setting properties and *in vitro* bioactivity *J. Mater. Sci., Mater. Med.* **20** 833–41

[43] Driessens F C M, Fernandez E, Ginebra M P, Boltong M G and Planell J A 1997 Calcium phosphates and ceramic bone cements vs. acrylic cements *An. De Quimica - Int. Ed.* **93** S38–43

[44] Driessens F C M, Planell J A and GIL X 1995 Calcium phosphates bone cements *Encyclopedic Handbook of Biomaterials and Bioengineering: Part B: Applications* ed D T D Wise *et al* (New York: CRC Press) pp 855–71

[45] Engstrand J, Persson C and Engqvist H 2014 The effect of composition on mechanical properties of brushite cements *J. Mech. Behav. Biomed. Mater.* **29** 81–90

[46] Machado J L M and Santos L A 2009 Production and use of paraffin microspheres for tissue scaffolds based on α-tricalcium phosphate cement *Ceramica* **55** 216–22

[47] Kokubo T, Kim H M and Kawashita M 2003 Novel bioactive materials with different mechanical properties *Biomaterials* **24** 2161–75

[48] Padilla S, Roman J, Sanchez-Salcedo S and Vallet-Regi M 2006 Hydroxyapatite/SiO_2-CaO-P_2O_5 glass materials: *In vitro* bioactivity and biocompatibility *Acta Biomaterialia* **2** 331–42

[49] Miguel B S *et al* 2010 Enhanced osteoblastic activity and bone regeneration using surface-modified porous bioactive glass scaffolds *J. Biomed. Mater. Res. Part* A **94A** 1023–33

[50] Takadama H and Kokubo T 2008 *In vitro* evaluation of bone bioactivity *Bioceramics and their Clinical Applications* ed T Kokubo (Cambridge: Woodhead) pp 165–82

[51] He Q *et al* 2012 Porous surface modified bioactive bone cement for enhanced bone bonding *Plos One* **7**
[52] Kaflak A and Kolodziejski W 2008 Kinetics of $^{1}H -> ^{31}P$ NMR cross-polarization in bone apatite and its mineral standards *Magn. Reson. Chem.* **46** 335–41
[53] Morejón-Alonso L, Carrodeguas R G and García-Menocal J A 2008 Transformations in CDHA/OCP/β-TCP scaffold during ageing in simulated body fluid at 36.5°C *J. Biomed. Mater. Res.* B **84** 386–93
[54] Li P J *et al* 1992 Apatite formation induced by silica-gel in a simulated body-fluid *J. Am. Ceram. Soc.* **75** 2094–7
[55] LeGeros R Z 1991 *Calcium Phosphates in Oral Biology and Medicine* (Basel: Karger) pp 46–67
[56] Hu G, Xiao L, Fu H, Bi D, Ma H and Tong P 2010 Study on injectable and degradable cement of calcium sulphate and calcium phosphate for bone repair *J. Mater. Sci., Mater. Med.* **21** 627–34
[57] Brown P W and Fulmer M 1991 Kinetics of hydroxyapatite formation at low temperature *J. Am. Ceram. Soc.* **74** 934–40
[58] Khairoun I, Boltong M G, Driessens F C M and Planell J A 1998 Some factors controlling the injectability of calcium phosphate bone cements *J. Mater. Sci., Mater. Med.* **9** 425–8
[59] dos Santos L A, Carrodéguas R G, Rogero S O, Higa O Z, Boschi A O and de Arruda A C F 2002 α-Tricalcium phosphate cement: '*in vitro*' cytotoxicity *Biomaterials* **23** 2035–42
[60] Franco R and Cidlowski J A 2009 Apoptosis and glutathione: beyond an antioxidant *Cell Death Differ.* **16** 1303–14
[61] Gulum M *et al* 2011 Sperm DNA damage and seminal oxidative status after shock-wave lithotripsy for distal ureteral stones *Fertil. Steril.* **96** 1087–90
[62] Altay M A, Erturk C, Kocyigit A, Taskin A and Celik H 2013 *In vitro* genotoxicity of calcium phosphate-based bone substitute material on human peripheral mononuclear leukocytes *Acta Medica Mediterranea* **29** 723–9
[63] de los Angeles Aguilar M, Pina M C, Lopez R M, Rodriguez L and Driessens F M 2005 Cytotoxic and genotoxic effects of the exposure of human lymphocytes to a calcium phosphate cement *in vitro J. Appl. Biomater. Biomech.* **3** 29–34
[64] Duan H W *et al* 2009 Biomarkers measured by cytokinesis-block micronucleus cytome assay for evaluating genetic damages induced by polycyclic aromatic hydrocarbons *Mutat. Res. Genet. Toxicol. Environ. Mutagen.* **677** 93–9
[65] Lindberg H K, Wang X, Jarventaus H, Falck G C M, Norppa H and Fenech M 2007 Origin of nuclear buds and micronuclei in normal and folate-deprived human lymphocytes *Mutat. Res./Fund. Mol. Mech. Mutagen.* **617** 33–45
[66] Chun B-D *et al* 2011 Interaction between odontoblast and bio-calcium phosphate cement reinforced with chitosan *J. Korean Assoc. Oral Maxillofaci. Surg.* **37** 415–20